

General Disclaimer

One or more of the Following Statements may affect this Document

- This document has been reproduced from the best copy furnished by the organizational source. It is being released in the interest of making available as much information as possible.
- This document may contain data, which exceeds the sheet parameters. It was furnished in this condition by the organizational source and is the best copy available.
- This document may contain tone-on-tone or color graphs, charts and/or pictures, which have been reproduced in black and white.
- This document is paginated as submitted by the original source.
- Portions of this document are not fully legible due to the historical nature of some of the material. However, it is the best reproduction available from the original submission.

X-641-69-150
PREPRINT

NASA TM X-63544

ELECTRON CAPTURE IN HIGHLY EVOLVED STARS

DAIICHIRO SUGIMOTO

N69-26682

FACILITY FORM 504

(ACCESSION NUMBER)

3

(PAGES)

TMX 63544

(NASA, CR OR TMX OR AD NUMBER)

(THRU)

30

(C/P/D/E)

(CATEGORY)

APRIL 1969



GODDARD SPACE FLIGHT CENTER
GREENBELT, MARYLAND

X-641-69-150
PREPRINT

ELECTRON CAPTURE IN HIGHLY EVOLVED STARS

Daiichiro Sugimoto*

NASA Goddard Space Flight Center, Greenbelt, Md.

April 1969

*NRC-NASA Resident Research Associate

GODDARD SPACE FLIGHT CENTER
Greenbelt, Maryland

PRECEDING PAGE BLANK NOT FILMED.

ELECTRON CAPTURE IN HIGHLY EVOLVED STARS

Daiichiro Sugimoto

NASA Goddard Space Flight Center, Greenbelt, Md.

ABSTRACT

When a star has evolved to a very high density (about $1 \times 10^9 \text{ g cm}^{-3}$), continuum electron capture by iron nuclei begins to play a role. Effects of electron capture upon gravitationally contracting iron stars of 1.4 and 2 solar masses have been investigated. As the electron capture process is rather slow compared with the dynamical time scale for the density below $10^{11} \text{ g cm}^{-3}$, it can be treated as an endothermic nuclear reaction. In spite of the absorption of energy by electron capture, the central temperature of the star is found to increase as the contraction of the star proceeds. For this phenomenon, the accompanying increase in the mean molecular weight is essential. Thus, a significant part of the star is found to enter into a region of temperature high enough for the photo-disintegration of iron to occur, before the star collapses by electron capture itself; the photo-disintegration commences at the center of a star of $2 M_{\odot}$, but in the outlying shells of a star of $1.4 M_{\odot}$.

ELECTRON CAPTURE IN HIGHLY EVOLVED STARS

I. INTRODUCTION

When a star has evolved to very high density (about $1 \times 10^9 \text{ g cm}^{-3}$), iron nuclei begin to capture continuum electrons. The nuclides in statistical equilibrium at given density and temperature have been computed by many authors (e.g., see Salpeter 1961; Tsuruta 1964). The results show that the most abundant nuclide in statistical equilibrium is not iron for densities above $1 \times 10^9 \text{ g cm}^{-3}$. Since the internal energy of the gas is absorbed in electron capture in many cases, and since the number of particles decreases, the value of the ratio of the specific heats for the quasi-static process, Γ_1 , can be less than 4/3 in this phase transition. This process has been postulated as a cause for dynamical instability in stars (Rakavy, Shaviv, and Zinamon 1967; Rakavy and Shaviv 1968).

The applicability of the notion of statistical equilibrium must be examined most carefully. A condition for statistical equilibrium is that the time scale of electron capture and its inverse reaction, i.e., beta decay or positron capture, should be shorter than the time scale of the phenomenon considered. For dynamical phenomena with a time scale of $(G\rho)^{-\frac{1}{2}}$, this condition requires a density greater than about $10^{11} \text{ g cm}^{-3}$ when electron capture by ^{56}Fe is fast enough. Thus, the notion of dynamical instability due to $\Gamma_1 < 4/3$ is not applicable below this density. Another condition for the attainment of statistical equilibrium is that the system is isolated. For a finite temperature there is beta decay through excited states, and energy is dissipated by neutrino pairs (URCA process). Thus, statistical equilibrium is realized in its exact meaning only for zero temperature, when beta decay is forbidden because of the high

Fermi energy of the electrons. For a finite temperature we must consider detailed balance between nuclides and electrons, together with energy loss by the URCA process.

In the present paper, we consider electron capture in iron stars with densities below 3×10^{10} g cm⁻³. It will be found that most of iron has captured electrons until the central density of the star reaches the above value. Thus the notion of the statistical equilibrium does not apply to our range of study.* The electron capture will be treated as an endothermic nuclear reaction in the sense that the internal energy of the gas is absorbed, and that the chemical composition is changed by this process. Details of the electron capture will be discussed in section II.

It is one of the main concerns in this paper to discover whether a star of given mass becomes unstable because of (i) the process of electron capture, (ii) iron-to-helium photo-disintegration, or (iii) general relativistic instability proposed by Chandrasekhar (1964). Though the actual chemical structure of the star is complicated, we simplify the problem by assuming an initially homogeneous iron star. For a star of mass less than the Chandrasekhar limit there is an upper limit for its central density and in only a relatively small mass range electron capture is important, according to the results of Finzi and Wolf (1967). We choose as two typical masses the values of 1.4 and 2 solar masses. The

*On the other hand, the rate of photo-disintegration is quite sensitive to temperature. For example the rates of (α, γ) reactions of ^{56}Fe and ^{28}Si , typical slow reactions, are both as fast as 8×10^3 sec⁻¹ at 5×10^9 °K according to interpolation formulae by Truran, Cameron, and Gilbert (1966). The dissociation of iron into helium and neutrons can be treated as in statistical equilibrium above such a temperature.

star of $1.4 M_{\odot}$ is above the Chandrasekhar limit for ^{56}Fe ($1.24 M_{\odot}$) or for ^{54}Fe ($1.33 M_{\odot}$), but below this limit for elements with equal numbers of protons and neutrons ($1.44 M_{\odot}$). Conditions in these stars will approximate those of the cores of more massive stars.

The structural change due to electron capture is analysed in section III in order to know its general features. The results of numerical computation are given in section IV. The main conclusion of the present study is that even for the star of $1.4 M_{\odot}$, the direct cause of dynamical instability is iron-to-helium dissociation, although it does not occur at the center of the star, but in outlying shells.

II. PHYSICAL DATA

a) Electron Capture

Bahcall (1964) has developed the theory of continuum electron capture in the stellar interior. Hansen (1966, 1968) has calculated the rates of electron capture as well as beta decay and other weak-interaction processes, taking into account excited states of nuclei. He has given interpolation formulae for various nuclides as functions of density for given temperatures. His result for the rates of electron captures by ^{56}Fe and ^{54}Fe , and of the beta decay of ^{56}Mn , are reproduced in Figure 1 together with the line of $(G\rho)^{-\frac{1}{2}}$, which is a measure of the dynamical time scale. We see that electron capture is a relatively slow process for the range of temperature and density given in this figure.

For the composition of the contracting star after silicon-burning phase, Fowler and Hoyle (1964) have developed a picture that ^{56}Ni is the principal nuclide just after silicon burning, when neutrino loss shortens the time scale of

silicon burning down to about 2×10^3 sec. Afterwards, ^{56}Ni gradually captures the continuum electrons to make the observed iron peak abundances. In our case of stars of relatively small mass, even the time scale of gravitational contraction after silicon burning is more than 10^4 sec (as will be shown in section IV), which is long enough for electron capture to make the iron peak. On the other hand, Truran, Cameron, and Gilbert (1966), and Bodansky, Clayton, and Fowler (1968) have studied in detail the nuclear transformation from ^{28}Si approaching nuclear statistical equilibrium at fixed temperatures and densities. In the case of density greater than 10^7 g cm^{-3} and of the life time more than 10^4 sec, the most abundant nuclide may be ^{54}Fe as pointed out first by Truran et al. (1966). Since they have not computed the above case up to the exhaustion of silicon, it is difficult to estimate what is the most abundant nuclide.

From the standpoint of stellar structure, the important parameters concerning electron capture are the following: (i) the rate of electron capture, (ii) the mean energy loss per capture, and (iii) the changes in mean molecular weights of electrons and of ions due to electron capture and the subsequent nuclear reactions. As illustrated in Figure 1, the rates for ^{56}Fe and ^{54}Fe are not substantially different except in the case of low temperatures and low densities where the difference in threshold energy is important. Thus, we consider only a star composed initially of pure ^{56}Fe , and adopt the capture rate of ^{56}Fe .

For the increase in mean molecular weight, we consider the cases of final products such as $^{84}_{34}\text{Se}$ and $^{56}_{24}\text{Cr}$. The ^{84}Se (Tsuruta 1964) was selected because of its magic neutron number, although the detailed transformation process is

unknown; ^{56}Cr was selected because it is an even-even nucleus. For the purpose of comparison, a third case was computed where only the absorption of energy was taken into account, but the change in mean molecular weight neglected (denoted as ^{56}Fe -to- ^{56}Fe).

In order to determine the energy absorption, we should know the detailed process of transformation including nuclear level structures. However, the difference of masses (Cameron and Elkin 1965) will be a measure of the energy absorption, i.e.,

$$(^{56}\text{Fe} + 26 e^-) - \frac{56}{84} (^{84}\text{Se} + 34 e^-) = -8.7 \text{ MeV/ } ^{56}\text{Fe}, \quad (1)$$

where e^- denotes the electron mass. The above value was applied even for the cases of ^{56}Cr and of ^{56}Fe . As this is a little too high a value in these cases, the result for the case of ^{56}Cr will give a higher central density for a given temperature. The real case will lie between the cases of ^{56}Cr and of ^{84}Se . When the Fermi energy becomes higher than the above value, the electrons near the top of Fermi sea will be absorbed to give a greater energy loss. Thus the rate of energy absorption can be written as

$$\epsilon_{ec} = \max \left\{ E_{Fe}, \left(\frac{Z_i}{A_i} - \frac{Z_f}{A_f} \right) (\psi + \sigma) \frac{kT}{M_o} \right\} X \lambda_{ec}, \quad (2)$$

where λ_{ec} denotes the rate of electron capture interpolated in Figure 1, X is the concentration by weight of ^{56}Fe , E_{Fe} is $1.5 \times 10^{17} \text{ erg g}^{-1}$ corresponding to the value in equation (1), Z and A are the charge and the mass numbers, respectively, the subscripts i and f denote initial (^{56}Fe) and final nuclides, and

M_e is the atomic mass unit. In equation (2), ψ and σ denote the chemical potential without the rest mass in units of kT , and the entropy in units of k , respectively, for one electron.

The change in the concentration of ^{56}Fe is described by

$$X(t + \Delta t) = X(t) - \left\{ X\lambda_{ec} - (1 - X)\lambda_\beta \right\}_t \Delta t, \quad (3)$$

where λ_β denotes the decay rate of ^{56}Mn . If strictly treated, the term $(1 - X)$ should be replaced by the concentration of ^{56}Mn . However, after numerical computation, the beta-decay term is found to be smaller than the electron-capture term in equation (3) at densities where the electron capture of ^{56}Mn is more rapid than its beta decay, i.e., the system is found to be far from electron-capture equilibrium.

b) Other Physical Data

Physical data used in the present study are, in principle, the same as those used by Murai, Sugimoto, Hoshi, and Hayashi (1968). However, several revisions have been made as described below.

Thermodynamical quantities.—Electrons, ions, and radiation have been taken into account, but the electron-positron pairs, which are of little importance for the mass range studied here, have been neglected. Thermodynamical quantities of ideal relativistic and partially degenerate electrons were numerically integrated and have been interpolated with an accuracy of better than 0.1 per cent. However, the electrostatic corrections (Salpeter 1961) were not taken into account.

Opacity.—The opacity adopted was that of Murai et al. (1968); it includes electron scattering, free-free, and relativistic electron conduction. Though Sampson (1961) has given interpolation formula of the electron scattering for temperatures up to 1.33×10^9 °K, the same expression has been used for even higher temperatures. The effect of electron degeneracy has been approximately included only by the available final states (Sampson 1961). The accuracy of the opacity is important only for the photon luminosity, L_{ph} , when extensive energy loss shortens the time scale of evolution.

Neutrino loss.—Throughout this paper, the term "neutrino loss" and the subscript ν denote the neutrino loss due to the direct weak interaction between electrons and neutrinos [$(\bar{\nu}) (\bar{e})$ interaction], and do not include neutrinos from electron capture and beta decay. The latter neutrinos are included in quantities with the subscript ec. Interpolation formulae for the neutrino loss rate given by Beaudet, Petrosian, and Salpeter (1967) have been used.

c) Effect of Change in Composition on Energy Conservation Equation

The equation for energy conservation can be written as

$$\frac{dL_r}{dM_r} = \epsilon_g - \epsilon_{ec} - \epsilon_\nu. \quad (4)$$

where L_r and ϵ_ν denote the heat flow and the neutrino loss rate, respectively. The energy release due to gravitational contraction, ϵ_g , is given by

$$-\frac{\epsilon_g}{T} dt = \frac{k}{\mu_i M_o} d \ln \frac{P_i^{3/2}}{\rho^{5/2}} + \frac{k}{\mu_e M_o} \left\{ d\sigma + (\psi + \sigma) d \ln \frac{1}{\mu_e} \right\} + ds_r, \quad (5)$$

where μ_i and μ_e denote the mean molecular weight of ions and of electrons, respectively, and where P_i and s_r are the ion pressure and the entropy density of radiation, respectively. The electron term in the curly brackets reduces to the same form as the ion term, when electrons are non-relativistic and non-degenerate. We notice that the right hand side is not the total derivative of the sum of the entropies of every constituent defined for statistical equilibrium. Such an expression (Kutter and Savedoff 1967) is valid only in the case of statistical equilibrium including nuclides, or in the case without any change in composition. In our case electron capture and beta decay are not in detailed balance.

d) Method of Computation

A Henyey type computational method has been used with about 40 mesh-points. The applicability of this method, when the time scale of evolution is short as compared with that of heat conduction, has been discussed in a separate paper (Sugimoto 1969). The inertia term has been neglected; since it opposes contraction as the contraction becomes faster and faster, the computation without it results in a contraction more rapid than the actual case. If the star were dynamically unstable, our method would not give any results, since the relaxation computation would not converge.

III. STRUCTURAL CHANGE DUE TO ELECTRON CAPTURE

From equations (2)-(5), we have

$$\frac{kT}{\mu_e M_o} \frac{d\sigma}{dt} = - \max \left\{ E_{Fe} - \left(\frac{Z_i}{A_i} - \frac{Z_f}{A_f} \right) (\psi + \sigma) \frac{kT}{M_o}, 0 \right\} X \lambda_{ec} - \epsilon_\nu, \quad (6)$$

where the term proportional to λ_β , and the ion and the radiation terms are

neglected, and where electron capture is assumed to proceed very rapidly as compared with heat conduction.

When the Fermi energy is high, the first term on the right hand side vanishes. When the neutrino loss rate is much less than the energy loss rate by electron capture, the entropy per electron remains nearly constant. That this is the situation may be seen in the following section.

In order to see the effect of a change in the mean molecular weight separately from the effect of energy loss, we consider a hypothetical case of electron capture of zero energy. Neglecting heat conduction, ion and radiation terms, and neutrino loss, we can put ϵ_g of equation (5) vanish and we then have

$$\frac{d\sigma}{d \ln \mu_e} = \psi + \sigma, \quad (6')$$

which means σ is increasing with μ_e . For a non-relativistic, non-degenerate gas, the right hand side of equation (6') reduces to $5/2$, which means that P^3/ρ^5 remains constant in time. By using this, we can solve the two differential equations of hydrostatic equilibrium of the star (involving dP/dM_r and dr/dM_r) separately from the other differential equations of the stellar structure. Thus, both P and ρ remain constant in time. This means that the temperature increases in proportion to the mean molecular weight.

This situation can be understood by using the virial theorem instead of equation (5). The virial theorem states that

$$3(\gamma - 1) U + \Omega = 0, \quad (7)$$

where the ratio of specific heats, γ , is assumed to be constant throughout the star, and where U and Ω denote the internal and the gravitational potential energy. The energy conservation for the whole star is written as

$$\frac{dE}{dt} = \frac{d(U + \Omega)}{dt} = -(3\gamma - 4) \frac{dU}{dT} = \frac{3 - 4}{\gamma - 1} \frac{d}{dt} \int_0^M \frac{kT}{\mu M_0} dV. \quad (8)$$

In the case of rapid electron capture of zero energy, E remains constant in the time scale considered, and there can be a solution in mechanical equilibrium where P and ρ remain constant throughout the star. Thus, T increases proportionally to μ .

IV. NUMERICAL RESULTS

Neglecting both neutrino loss and electron capture, the evolution of the contracting iron stars was computed, beginning with a polytrope of index 3 at the temperature of helium-burning. A particular stage of this computation was then used as the initial structure for computation, including the electron-capture process. The central temperatures and densities ($\log T_c$ [$^{\circ}$ K], $\log \rho_c$ [g cm^{-3}]) assumed for the initial structures were (9.522, 8.220) for the star of $1.4 M_{\odot}$, and (9.513, 7.507) for $2 M_{\odot}$. The stellar structures at these stages are similar to the polytrope of index 3, $P \sim \rho^{4/3}$, though $\rho \sim T^3$ does not hold because of weak degeneracy of the electrons. At these temperatures the energy-generation rate due to silicon burning (Bodansky et al. 1968) is approximately of the same order of magnitude as the neutrino loss rate. Thus the above conditions will pertain to a point just after the silicon-burning phase.

Savedoff, VanHorn, and Vila (1968) have computed the evolution of contracting iron stars starting from the temperature of helium burning. They have taken into account neutrino loss throughout the contraction, and have obtained higher central density than the contracting star without neutrinos. However, the evolutionary track of the central temperature and density depends upon initial condition of contraction, since the entropy distribution through the star is nearly frozen beyond the temperature of carbon burning because of extensive neutrino loss. Since the iron core will be formed in an isentropic convection core in the silicon-burning phase, the structure of the polytrope of index 3 or the contracting star without neutrinos will approximate the structure just after the silicon-burning phase better than their iron stars (Sugimoto 1969a).

Tables 1-3 give the results for the star of $1.4 M_{\odot}$ for the cases of ^{56}Fe -to- ^{84}Se , ^{56}Fe -to- ^{56}Cr , and ^{56}Fe -to- ^{56}Fe , respectively. Tables 4 and 5 give the results for the star of $2 M_{\odot}$ for the cases ^{56}Fe -to- ^{84}Se , and ^{56}Fe -to- ^{56}Fe . The e-folding time of the central density is compared with the time scale of free fall in the second column. The energy loss due to neutrinos produced by electron capture, and to the decrease in the total binding energy of the nuclei are expressed by $L_{ec} = \int_0^M \epsilon_{ec} dM_r$. A case where the direct interaction between electrons and neutrinos (L_{ν}) is neglected, is given in Table 6 for the case of ^{56}Fe -to- ^{84}Se for the star of $1.4 M_{\odot}$.

Evolutionary tracks of the centers of the stars are shown in the temperature-density diagram of Figures 2 and 3 for 1.4 and $2 M_{\odot}$, respectively. Additionally, in Figure 2 the temperature-density distributions (structure lines) through the star of $1.4 M_{\odot}$ are illustrated for particular evolutionary stages, where the time

scale of contraction is nearly equal to that of free fall. Except for the ^{56}Fe -to- ^{56}Fe case for $1.4 M_{\odot}$, the central temperature rises as the contraction proceeds. The value of σ_c is nearly constant after L_{ec} has exceeded L_{ν} . A slight increase in σ_c in the latest stages comes from the term involving the entropy of ions. In the ^{56}Fe -to- ^{56}Fe case for $1.4 M_{\odot}$, the central temperature decreases monotonically. For the star of $2 M_{\odot}$ the central temperature increases even in the ^{56}Fe -to- ^{56}Fe case, because of its large mass as compared with the Chandrasekhar limit.

For the star of $2 M_{\odot}$ the temperature is maximum at the center throughout all evolutionary stages, and the center of the star enters the iron-to-helium photo-disintegration region. (Neither the photo-disintegration is taken into account in the computation, nor the plasma effect (Bodansky et al. 1968) is taken into account in the lines of constant abundance of iron in Figures 2 and 3.) On the other hand, for $1.4 M_{\odot}$ the point of the maximum temperature throughout the star lies in an outer shell. For the three models illustrated by the structure lines in Figure 2, the maximum temperature lies at the mass fraction $M_r/M \approx 0.25 \sim 0.3$, and a major part of the star ($0.8 \lesssim M_r/M \lesssim 0.7$) has already entered into the photo-disintegration region.

In the ^{56}Fe -to- ^{56}Fe case for $1.4 M_{\odot}$, the point of the maximum temperature lies at $\log T = 9.61$, $\log \rho = 8.52$, and $M_r/M = 0.48$, when the central density is $\log \rho_c = 9.258$ (stage 5 in Table 3). On the other hand, the temperature and density of the ^{56}Fe -to- ^{84}Se case for the star of $1.4 M_{\odot}$ (Table 1) are $\log T = 9.62$ and $\log \rho = 8.45$ at the same mass fraction of the star at a stage with the same central density as the above case. These conditions are only slightly different

between the above two cases in spite of a great difference in the central temperatures. In view of this and the proximity of the structure lines in shells exterior of the maximum temperatures (Figure 2), the contraction of the outer shells, where electron capture proceeds much more slowly as compared with at the center, depends but slightly upon the details of the electron-capture process.

In the case where neutrino loss is neglected, the central temperature is lower than in the other cases of the same central density. In that case the entropy-density gradient is produced only by the energy loss due to electron capture. So at the early stage of electron capture, the stronger gradient is produced near the center because of its density dependence. The stronger entropy-density gradient results in higher central density.

The distributions of the iron which has not yet captured electrons are illustrated in Figures 4 and 5. The iron is consumed in a rather wide region of the core except for the case of ^{56}Fe -to- ^{84}Se for $2 M_{\odot}$. This comes from the fact that the temperature gradient is small or even inverted, and the rate of electron capture is not much different throughout such a region. Most of iron has captured electrons at the center before the rate of contraction becomes nearly that of free fall. However, if electron capture were in detailed balance with beta decay, the concentration of the iron at the center would be much smaller, i.e., as small as 10^{-4} and 5×10^{-2} for the last stages of 1.4 and $2 M_{\odot}$ stars, respectively, as may be seen in Figure 1.

V. SUMMARY AND DISCUSSION

The general features of contraction with electron capture are as follows. Because of the change in mean molecular weight, the central temperature rises

as electron capture proceeds, even when the electrons are rather strongly degenerate, as seen in section IV and as discussed in section III. The reason is that the energy required by electron capture is supplied not only by the thermal energy of the order of σkT but also by ψkT , the Fermi energy of the degenerate electrons. If we have to select a more relatively neutron rich nucleus than ^{84}Se , the central temperature will be higher, at a given value of the central density than would be the case for ^{84}Se .

The above results are quite general in the following sense. When $(\psi + \sigma)kT$ becomes more than the threshold energy for electron capture, the above result is applicable even for a different element, if only the time scale of contraction, which is essentially determined by the rate of electron capture, is suitably altered. In this case the amount of absorbed energy is determined essentially by the energy of electron, even if a more detailed process of electron capture on a different element, such as ^{54}Fe , were taken into account.

The threshold for electron capture by ^{32}S is especially low, ~ 1.5 MeV, and its electron capture is effective for densities above 10^8 g cm^{-3} (Salpeter 1961). Before the silicon-burning phase, it will affect the detailed network of nuclear burning reactions. The abundance of ^{32}S , which is produced within the silicon-burning phase, is rather large according to Truran et al. (1966) and Bodansky et al. (1968); however, the abundance remaining after silicon burning is at present open to question. In view of the fact that most of the iron captures electrons before capture rate becomes rapid as compared with the free-fall time, and that the electron capture makes the central temperature higher, the phase of electron capture by ^{32}S will be passed by without any serious effect upon the later evolutionary phases.

Thus, we may conclude that the iron star of mass $M \gtrsim 1.4 M_{\odot}$ becomes unstable due to the photo-disintegration of iron or heavier elements produced by electron capture. For stars of small mass, the instability commences not always at the center of the star but in an outlying shell. The temperature necessary for photo-disintegration of the heavier nuclides is lower than that of iron. General relativistic instability will occur at a central density above about $2.3 \times 10^{10} \text{ g cm}^{-3}$ (Chandrasekhar and Topper 1964). Before this central density the star has become unstable by the photo-disintegration.

The star of $M \lesssim 1.4 M_{\odot}$ was below the Chandrasekhar limit when it was composed of an element with equal numbers of proton and neutrons, and it would not burn silicon. Even if there is a phase of silicon burning resulting from a complex chemical structure in an actual star, the silicon burning itself will nevertheless be considerably modified by the effects of electron capture.

ACKNOWLEDGMENT

The author wishes to thank Dr. T. G. Northrop for his stay at the Goddard Space Flight Center as a resident research associate of NRC-NASA. Thanks are also due to Drs. R. C. Cameron and T. Kelsall for encouragement, discussion, and reading of the manuscript. Numerical computations were made with IBM 360/91 at the Goddard Space Flight Center.

REFERENCES

Bahcall, J. N. 1964, Ap. J., 139, 318.

Beaudet, G., Petrosian, V., and Salpeter, E. E. 1967, Ap. J., 150, 979.

Bodansky, D., Clayton, D. D., and Fowler, W. A. 1968, Ap. J. Suppl., 16, 299
(No. 148).

Cameron, A. G. W., and Elkin, R. M. 1965, Canadian J. Phys., 43, 1288.

Chandrasekhar, S. 1964, Ap. J., 140, 417.

Chandrasekhar, S., and Topper, R. F. 1964, Ap. J., 139, 1396.

Finzi, A., and Wolf, R. A. 1967, Ap. J., 150, 115.

Fowler, W. A., and Hoyle, F. 1964, Ap. J. Suppl., 9, 201 (No. 91).

Hansen, C. L. 1966, Thesis, Yale Univ. (unpublished).

_____. 1968, Ap. and Space Sci., 1, 499.

Kutter, G. S., and Savedoff, M. P. 1967, A. J., 72, 810.

Murai, T., Sugimoto, D., Hōshi, R., and Hayashi, C. 1968, Progr. Theor. Phys.
(Kyoto), 39, 619.

Rakavy, G., Shaviv, G., and Zinamon, Z. 1967, Ap. J., 150, 131.

Rakavy, G., and Shaviv, G. 1968, Ap. and Space Sci., 1, 429.

Salpeter, E. E. 1961, Ap. J., 134, 669.

Sampson, D. H. 1961, Ap. J., 134, 482.

Savedoff, M. P., VanHorn, H. M., and Vila, S. C. 1969, Ap. J., 155, 221.

Sugimoto, D. 1969, to be submitted for publication.

_____. 1969a, to be published in Bull. Amer. Astron. Soc.

Truran, J. W., Cameron, A. G. W., and Gilbert, A. Canadian J. Phys., 44, 563.

Tsuruta, S. 1964, thesis, Columbia Univ. (unpublished).

TABLE 1

CONTRACTION OF A 1.4 M_{\odot} STAR WITH ELECTRON CAPTURE FROM ^{56}Fe TO $^{84}\text{Se}^*$

Stage	$(G\rho_f)^{\frac{1}{2}} \times \frac{dt}{d\rho} \ln \rho_c$	X_c	$\log \rho_c$	$\log T_c$	ψ_c	σ_c	L_{ec}/L_{\odot}	L_{ν}/L_{\odot}	L_{ph}/L_{\odot}
1	9.2(5)	1.000	8.238	9.522	5.76	1.262	7.99(9)	2.84(10)	6.39(3)
2	9.3(5)	0.861	8.476	9.489	7.92	0.987	3.14(10)	2.74(10)	8.23(3)
3	1.6(5)	0.506	8.816	9.524	9.85	0.836	3.96(11)	6.97(10)	1.17(4)
4	6.2(4)	0.369	8.956	9.556	10.3	0.813	1.35(12)	1.23(11)	1.34(4)
5	7.9(2)	0.118	9.467	9.686	11.7	0.747	1.72(14)	1.15(12)	2.23(4)
6	1.5(2)	0.065	9.815	9.787	12.4	0.722	7.01(15)	5.42(12)	3.14(4)
7	4.9(0)	0.048	9.995	9.847	12.5	0.722	6.09(16)	1.23(13)	3.73(4)
8	4.7(-1)	0.038	10.183	9.910	12.6	0.724	7.23(17)	2.92(13)	4.45(4)

* Throughout Tables, the number in parentheses is the power of 10 by which the associated tabular number is to be multiplied, and the subscript c denotes values at the center.

TABLE 2
CONTRACTION OF A $1.4 M_{\odot}$ STAR WITH ELECTRON CAPTURE FROM ^{56}Fe TO ^{56}Cr

Stage	$\times \frac{(G\rho_c)^{\frac{1}{2}}}{dt/d\ln\rho_c}$	X_c	$\log \rho_c$	$\log T_c$	ψ_c	σ_c	L_{ec}/L_{\odot}	L_{ν}/L_{\odot}	L_{ph}/L_{\odot}
1	9.4(5)	1.000	8.238	9.522	5.76	1.262	7.99(9)	2.84(10)	6.39(3)
2	1.0(6)	0.860	8.481	9.473	8.30	0.946	3.02(10)	2.61(10)	8.30(3)
3	1.7(5)	0.501	8.879	9.454	12.5	0.675	4.41(11)	7.42(10)	1.27(4)
4	5.4(4)	0.362	9.060	9.478	13.8	0.622	1.80(12)	1.51(11)	1.53(4)
5	5.1(3)	0.176	9.398	9.563	15.1	0.586	3.25(13)	6.54(11)	2.17(4)
6	3.1(2)	0.083	9.758	9.666	16.0	0.564	1.10(15)	3.29(12)	3.11(4)
7	3.6(1)	0.061	9.957	9.729	16.3	0.559	9.60(15)	8.06(12)	3.77(4)
8	3.9(0)	0.047	10.135	9.789	16.4	0.560	8.28(16)	1.83(13)	4.47(4)

TABLE 3

CONTRACTION OF A $1.4 M_{\odot}$ STAR WITH ELECTRON CAPTURE FROM ^{56}Fe TO ^{56}Fe

Stage	$\times \frac{(G\rho_c)^{\frac{1}{2}}}{dt/d \ln \rho_c}$	X_c	$\log \rho_c$	$\log T_c$	ψ_c	σ_c	$L_{\odot c}/L_{\odot}$	L_{ν}/L_{\odot}	L_{ph}/L_{\odot}
1	9.6(5)	1.000	8.238	9.522	5.76	1.262	7.99(9)	2.84(10)	6.39(3)
2	1.2(6)	0.868	8.476	9.451	8.76	0.902	2.66(10)	2.42(10)	8.29(3)
3	4.8(5)	0.659	8.766	9.331	15.3	0.660	1.31(11)	4.15(10)	1.15(4)
4	1.7(5)	0.542	9.003	9.180	26.9	0.324	5.57(11)	8.85(10)	1.49(4)
5	4.1(4)	0.465	9.258	8.735	93.5	0.096	3.06(12)	2.30(11)	1.96(4)

TABLE 4

CONTRACTION OF A 2 M_{\odot} STAR WITH ELECTRON CAPTURE FROM ^{56}Fe TO ^{84}Se

Stage	$\times \frac{(G\rho_c)^{\frac{1}{2}}}{dt/d \ln \rho_c}$	X_c	$\log \rho_c$	$\log T_c$	ψ_c	σ_c	L_{ec}/L_{\odot}	L_{ν}/L_{\odot}	L_{ph}/L_{\odot}
1	4.2(4)	1.000	7.531	9.517	2.37	2.11	1.52(8)	5.03(11)	5.49(4)
2	2.8(4)	0.998	8.019	9.601	3.58	1.75	1.53(10)	1.87(12)	7.10(4)
3	1.5(4)	0.976	8.294	9.664	4.13	1.64	2.39(11)	4.54(12)	8.30(4)
4	5.8(3)	0.847	8.580	9.736	4.59	1.56	4.17(12)	1.22(13)	9.76(4)
5	1.3(3)	0.572	8.832	9.802	4.92	1.51	5.39(13)	3.05(13)	1.11(5)
6	1.1(2)	0.243	9.128	9.886	5.19	1.48	1.26(15)	9.67(13)	1.30(5)

TABLE 5

CONTRACTION OF A 2 M_⦿ STAR WITH ELECTRON CAPTURE FROM ⁵⁶Fe TO ⁵⁶Fe

Stage	$\frac{(G\rho_e)^{\frac{1}{2}}}{dt/d \ln \rho_e}$	X_c	$\log \rho_c$	$\log T_c$	ψ_c	σ_c	L_{e^c}/L_{\odot}	L_{ν}/L_{\odot}	L_{ph}/L_{\odot}
1	4.2(4)	1.000	7.531	9.517	2.37	2.11	1.52(8)	5.03(11)	5.49(4)
2	3.1(4)	0.998	7.982	9.592	3.50	1.77	1.05(10)	1.66(12)	6.95(4)
3	6.0(3)	0.859	8.601	9.720	4.95	1.48	4.38(12)	1.26(13)	9.93(4)
4	2.0(3)	0.649	8.842	9.755	5.79	1.33	3.52(13)	2.88(13)	1.14(5)
5	3.7(2)	0.401	9.124	9.799	6.80	1.19	3.97(14)	8.03(13)	1.34(5)
6	4.3(1)	0.227	9.399	9.858	7.57	1.11	5.30(15)	2.33(14)	1.57(5)
7	4.2(0)	0.127	9.642	9.923	8.01	1.07	7.45(16)	6.22(14)	1.83(5)

TABLE 6
CONTRACTION OF A $1.4 M_{\odot}$ WITH ELECTRON CAPTURE FROM ^{56}Fe TO ^{84}Se WITHOUT NEUTRINO LOSS

Stage	$\frac{(G\rho_e)^{\frac{1}{2}}}{dt/d \ln \rho_e}$	X_c	$\log \rho_c$	$\log T_c$	ψ_c	σ_c	L_{ec}/L_{\odot}	L_{ν}/L_{\odot}	L_{ph}/L_{\odot}
1	3.7(6)	1.000	8.240	9.513	5.90	1.238	7.68(9)	-	6.39(3)
2	2.8(6)	0.851	8.492	9.387	10.3	0.776	1.96(10)	-	8.13(3)
3	4.1(5)	0.571	8.806	9.406	13.0	0.643	1.89(11)	-	1.12(4)
4	3.1(4)	0.356	9.156	9.468	15.2	0.572	4.66(12)	-	1.61(4)
5	3.1(3)	0.282	9.393	9.517	16.5	0.535	4.96(13)	-	2.05(4)
6	9.5(2)	0.221	9.751	9.614	17.8	0.509	2.40(15)	-	2.93(4)
7	3.2(0)	0.197	10.043	9.711	18.0	0.509	8.77(16)	-	3.89(4)
8	8.1(-1)	0.192	10.155	9.751	18.0	0.511	4.05(17)	-	4.32(4)

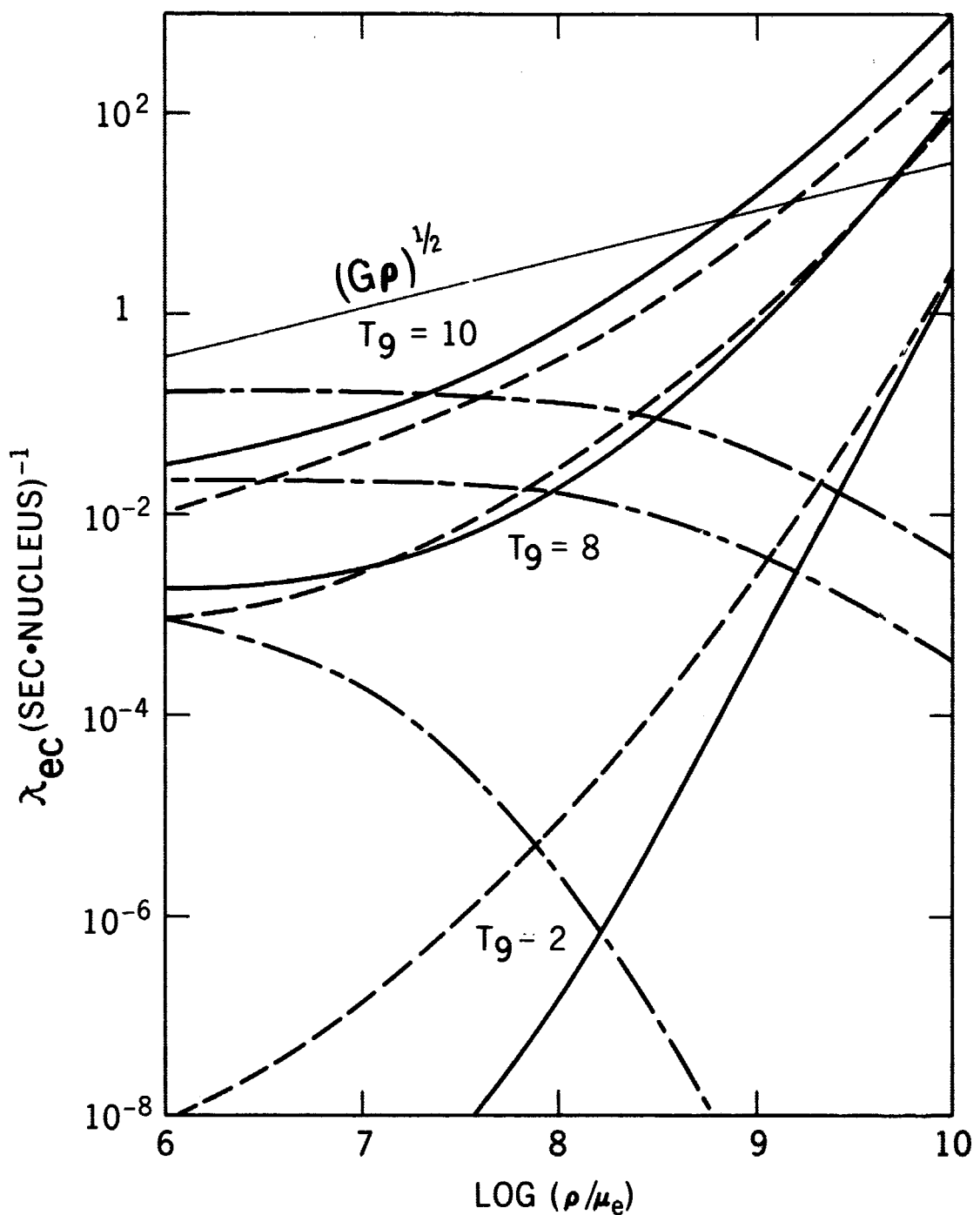


Figure 1. Rates of electron capture of ^{56}Fe (solid curves) and of ^{54}Fe (dashed), and rates of beta decay of ^{56}Mn (dash-dot) for given temperatures (in units of 10^9 °K) as indicated (Hansen 1966; 1968). The reciprocal of the time scale of free fall, $(G\rho)^{1/2}$, is shown by a thin straight line.

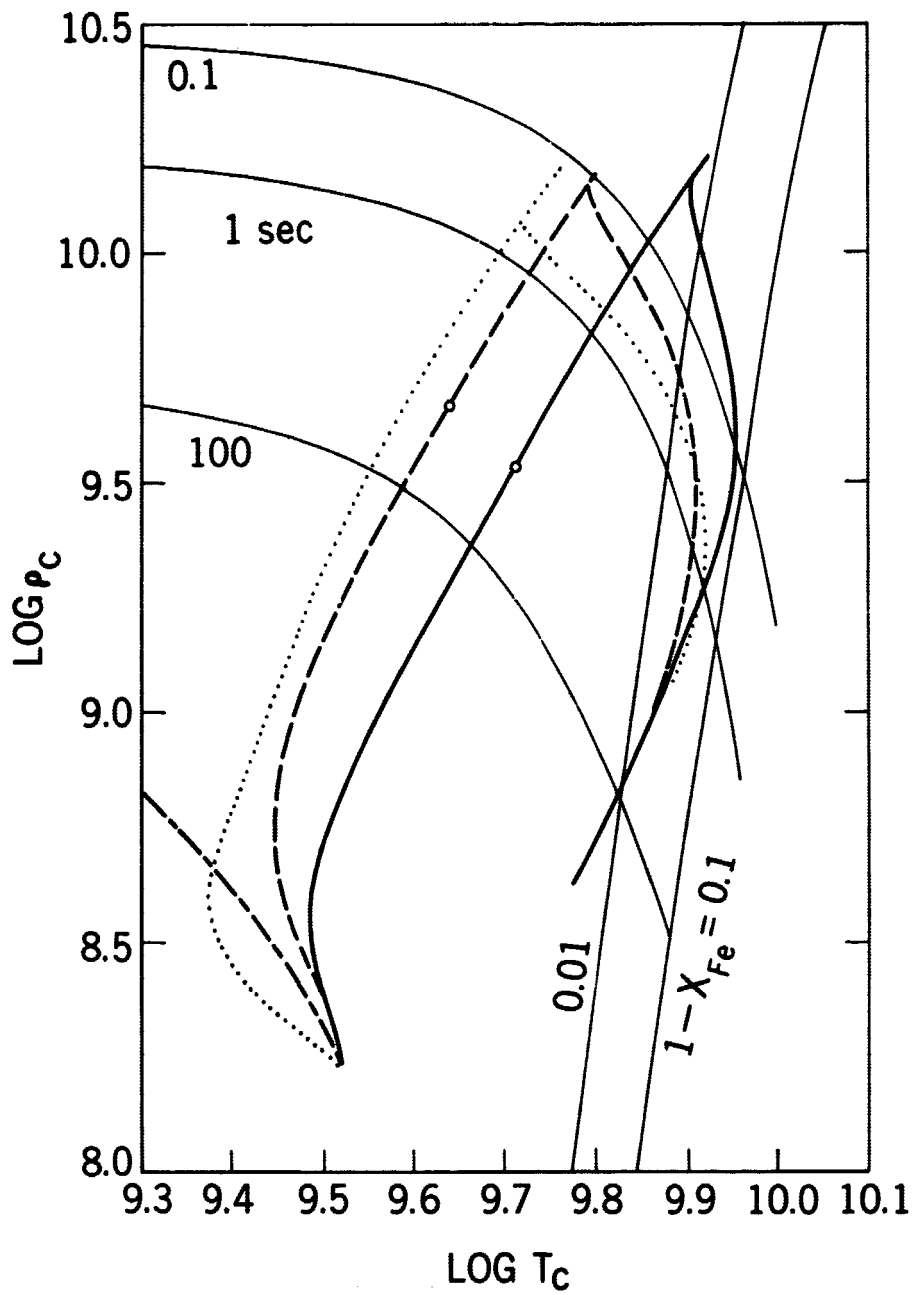


Figure 2. Evolutionary paths of the center of a star of $1.4 M_{\odot}$ for the cases of ^{56}Fe -to- ^{84}Se (solid curve on the left side), ^{56}Fe -to- ^{56}Cr (dashed), ^{56}Fe -to- ^{56}Fe (i.e., with change in mean molecular weight neglected), and ^{56}Fe -to- ^{84}Se without neutrino loss (dotted). Circles on these curves indicate stages where 90 per cent of the iron has captured electrons at the center. Curves on the right-hand side are structure lines extending from the center to the surface of the star for particular stages. Superposed are thin curves of loci of constant electron-capture lifetimes of ^{56}Fe and loci of constant abundance of iron in statistical equilibrium with helium and neutrons.

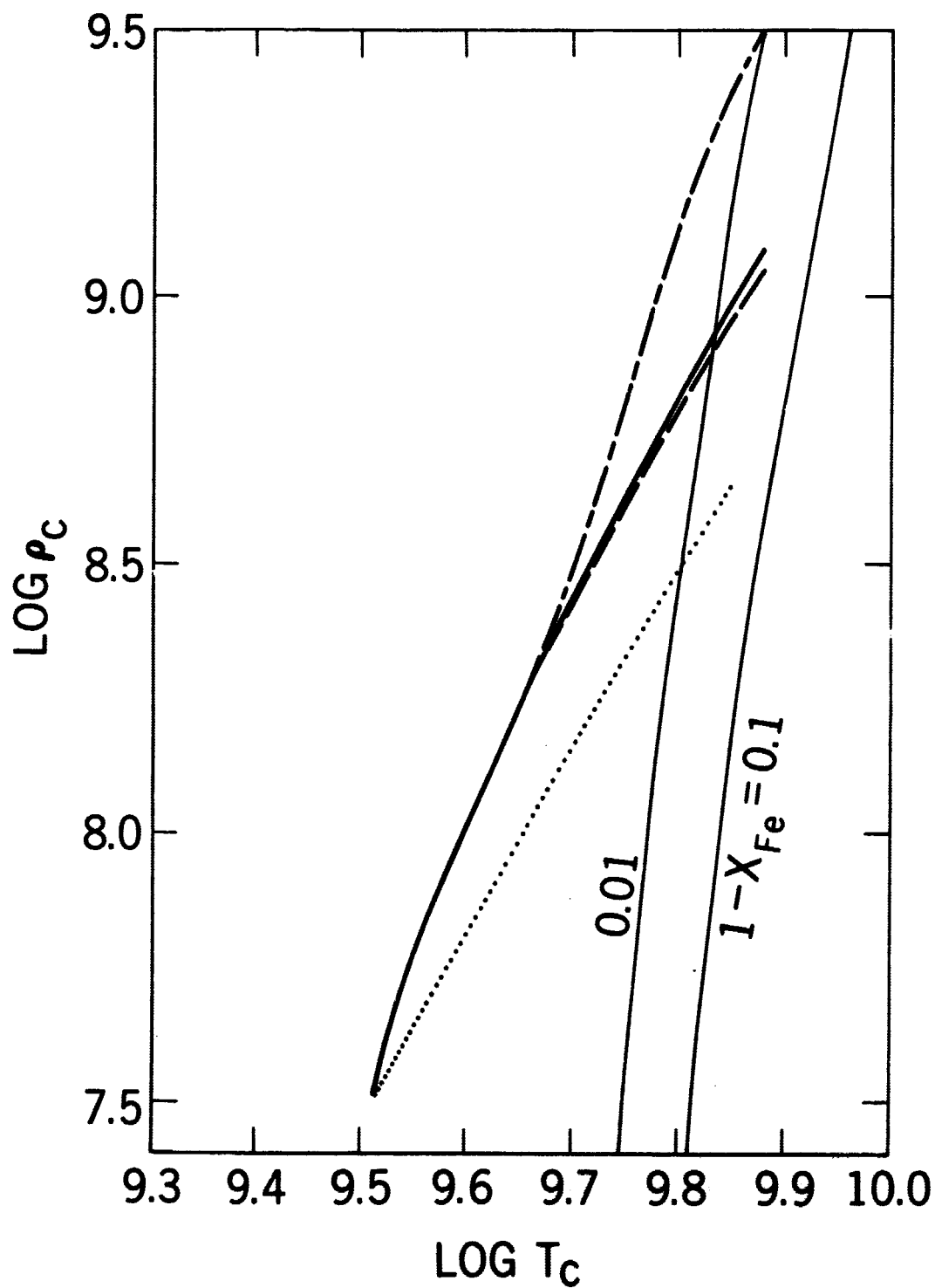


Figure 3. The same as Figure 2, but for $2 M_{\odot}$ for the cases from ^{56}Fe -to- ^{84}Se (solid curve), and ^{56}Fe -to- ^{56}Fe (dash-dot). Evolutionary paths of the center without electron capture (dashed line) and with neither the electron capture nor neutrino loss are added for comparison.

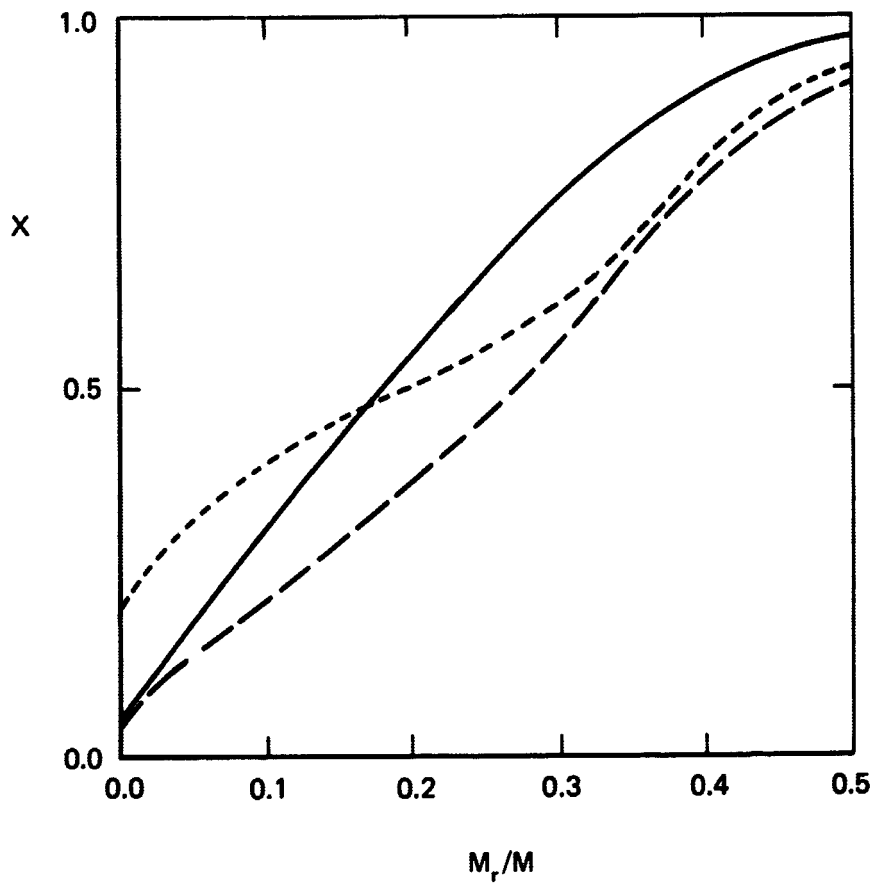


Figure 4. Distribution of the iron, which has not yet captured electrons in the stars of $1.4 M_{\odot}$ for stages 8 of Table 1 (solid curve), of Table 2 (dashed), and of Table 6 (dotted).

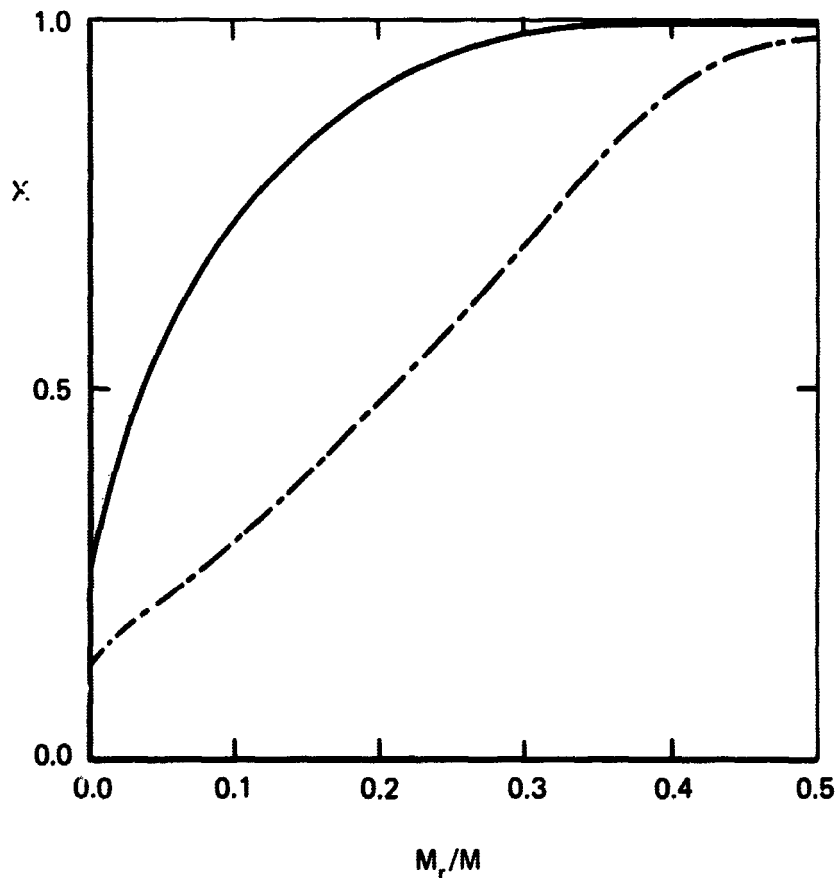


Figure 5. The same as Figure 4, but for $2 M_{\odot}$, for stage 6 of Table 4 (solid curve), and stage 7 of Table 5 (dash-dot).